2D IR spectroscopy of high-pressure phases of ice

Halina Tran, Ana V. Cunha, Jacob J. Shephard, Andrey Shalit, Peter Hamm, Thomas L. C. Jansen, and Christoph G. Salzmann

Citation: The Journal of Chemical Physics **147**, 144501 (2017);

View online: https://doi.org/10.1063/1.4993952

View Table of Contents: http://aip.scitation.org/toc/jcp/147/14

Published by the American Institute of Physics

2D IR spectroscopy of high-pressure phases of ice

Halina Tran,[1,a)] Ana V. Cunha,[2,a)] Jacob J. Shephard,[3] Andrey Shalit,[1]
Peter Hamm,[1,b)] Thomas L. C. Jansen,[2,b)] and Christoph G. Salzmann[3,b)]
[1]*Department of Chemistry, University of Zürich, Zürich, Switzerland*
[2]*Zernike Institute for Advanced Materials, University of Groningen, Groningen, The Netherlands*
[3]*Department of Chemistry, University College London, 20 Gordon Street, London WC1H 0AJ, United Kingdom*

(Received 3 July 2017; accepted 30 August 2017; published online 10 October 2017)

We present experimental and simulated 2D IR spectra of some high-pressure forms of isotope-pure D_2O ice and compare the results to those of ice I*h* published previously [F. Perakis and P. Hamm, Phys. Chem. Chem. Phys. **14**, 6250 (2012); L. Shi *et al.*, *ibid.* **18**, 3772 (2016)]. Ice II, ice V, and ice XIII have been chosen for this study, since this selection covers many aspects of the polymorphism of ice. That is, ice II is a hydrogen-ordered phase of ice, in contrast to ice I*h*, while ice V and ice XIII are a hydrogen-disordered/ordered couple that shares essentially the same oxygen structure and hydrogen-bonded network. For the transmission 2D IR spectroscopy, a novel method had to be developed for the preparation of ultrathin films (1-2 μm) of high-pressure ices with good optical quality. We also simulated 2D IR spectra based on molecular dynamics simulations connected to a vibrational exciton picture. These simulations agree with the experimental results in a semi-quantitative manner for ice II, while the same approach failed for ice V and ice XIII. From the perspective of 2D IR spectroscopy, ice II appears to be more inhomogeneously broadened than ice I*h*, despite its hydrogen-order, which we attribute to the fact that ice II is structurally more complex with four distinguishable hydrogen bonds that mix due to exciton coupling. Ice V and ice XIII, on the other hand, behave as expected with the hydrogen-disordered case (ice V) being more inhomogenously broadened. Furthermore, in all hydrogen-ordered forms (ice II and ice XIII), cross peaks could be identified in the anisotropic 2D IR spectrum, whose signs reveal the relative direction of the corresponding excitonic states. *Published by AIP Publishing.* https://doi.org/10.1063/1.4993952

I. INTRODUCTION

The water molecule displays enormous structural complexity in its condensed forms including the highly anomalous liquid phase,[1,2] seventeen crystalline phases of ice,[3–5] at least two families of amorphous ices,[6–8] and stacking-disordered ice, which displays crystalline order in only two dimensions.[9–11] The crystalline phases of ice can be categorized with respect to the degree of orientational order the water molecules display. As shown in Fig. 1(a), the fully hydrogen-bonded water molecules in ice can in principle adopt six different orientations. In hydrogen-disordered phases of ice, such as the well-known "ordinary" hexagonal ice I*h*, all six orientations are realized. The average structure, as determined by neutron diffraction, consequently shows two half-occupied hydrogen sites along each of the hydrogen bonds.[12] As required by the 3rd law of thermodynamics, the hydrogen-disordered ices are expected to transform to their corresponding hydrogen-ordered counterparts at low temperatures and the water molecules are found in only one of the six orientations.[3]

Vibrational spectroscopy has proven to be an invaluable tool for studying the complex structures and dynamics of water, ice, and aqueous systems in general.[13–15] However, water is notorious for displaying broad and overlapping spectroscopic features which arise from complicated intermolecular coupling processes of the O—H oscillators and can make peak assignments and structural interpretations difficult. A particular challenging question in this context is how the structural disorder of hydrogen-bonded water networks affects the extent and spatial distance over which coupling takes place and how these effects manifest in the spectra. The hydrogen-ordered phases of ice represent an important class of materials in this respect since they are the only forms of condensed water for which the spectroscopic selection rules are firmly defined[16] and consequently, coupling processes are expected to take place over very long distances.

In order to obtain a more complete understanding of the spectroscopy of condensed water phases, multi-dimensional spectroscopic techniques have been recently employed to study isotope-diluted[17–19] and isotope-pure ice I*h*[20,21] both experimentally and theoretically. 2D IR spectroscopy extends conventional IR absorption spectroscopy, which is also sometimes called linear or 1D spectroscopy, by an extra frequency dimension. Thereby, 2D IR spectroscopy correlates a "pump spectrum" with a "probe spectrum," the measurement of which might be separated by a time delay that we will call population time. Since the water molecules in the ice crystal are densely packed, the OH (or OD) vibrations of neighboring molecules are strongly coupled, mostly via

[a)]H. Tran and A. V. Cunha contributed equally to this work.
[b)]Authors to whom correspondence should be addressed: peter.hamm@chem.uzh.ch, t.l.c.jansen@rug.nl, and c.salzmann@ucl.ac.uk

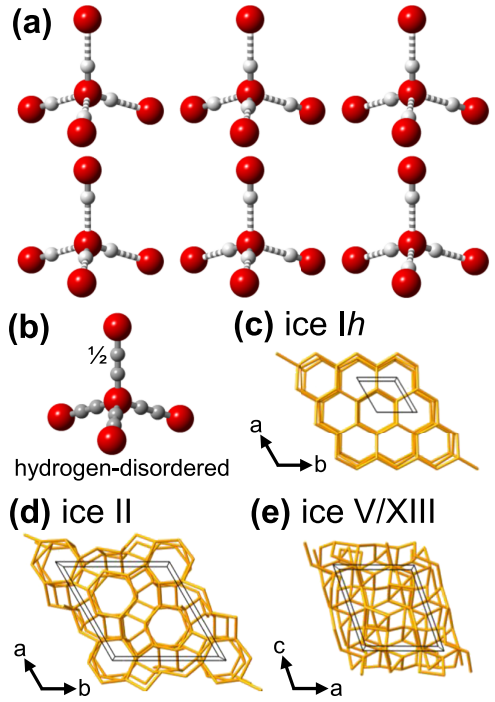

FIG. 1. (a) Six possible orientations of a water molecule in ice. Oxygen and hydrogen atoms are represented by red and white spheres, respectively. Covalent O—H bonds are indicated by solid and O···H hydrogen bonds are indicated by dashed lines. (b) Average hydrogen-disordered structure with half-occupied hydrogen positions. Hydrogen-bond networks of (c) ice I*h*, (d) ice II, and (e) ice V/XIII. The nodes of the networks represent the oxygen atoms and the lines the hydrogen bonds, respectively. The ice II structure is shown with its hexagonal unit cell[42,43] and the unit cell of the ice V/XIII network with the centering of the $P2_1/a$ space group of ice XIII.[46]

Coulombic interactions.[22,23] We will refer to this mechanism as "excitonic coupling," and in fact, 2D IR spectroscopy started out by observing exactly these excitonic couplings for the C=O (amide I) vibrations in a protein.[24] In isotope-pure liquid water, random exciton coupling leads to broad line shapes and very fast relaxation in the 2D IR response.[25,26] On the other hand, for isotope-pure ices, it is generally accepted that exciton coupling is the reason for their peculiar and complex spectra.[21–23,27] Since the strength of excitonic coupling depends on the relative distance and orientation of the water molecules in an ice crystal, the coupling pattern is determined by the crystal structure. While excitonic coupling does affect the 1D lineshape of an IR absorption spectrum, it does so in a way that the problem cannot be inverted, i.e., one cannot deduce the coupling Hamiltonian uniquely from a 1D spectrum. On the other hand, excitonic coupling causes cross peaks in a 2D IR spectrum. It is that additional information which enables one to uniquely invert the problem, at least in idealized situations.[28] And indeed, spectral simulations based on an excitonic coupling Hamiltonian did reveal almost quantitative agreement with experimental 1D[22,23] as well as 2D IR[21] spectra of ice I*h*.

Another piece of information, which can be extracted only from 2D IR spectra and not from 1D absorption spectra, concerns the amount of inhomogeneous broadening.[29–31] If a spectroscopic transition is inhomogenously broadened, for example, due to hydrogen-disorder or presence of different hydrogen-bond environments, the corresponding 2D IR peak will be elongated along the diagonal. While such an elongation could be observed for isotope-diluted ice I*h* both in experiment[19] and simulation,[18] the 2D IR spectra of neat ice I*h* did not reveal any signature of inhomogeneous broadening,[20] suggesting a strong exchange narrowing effect.[18] This exchange narrowing arises from the previously discussed excitonic coupling between local vibrations leading to the formation of delocalized states which essentially report on an average of the frequencies of the involved local vibrations. In liquid water, delocalization is over about ten OD-stretches,[32] while in ice I*h* one order of magnitude more local modes were reported to be involved.[22] This coupling further leads to multiple such delocalized states. For neat ice I*h*, three of these states were identified.[23] In the isotropic 2D IR spectra, strong cross peaks were found both in theory and experiment, which were assigned to arise due to the formation of delocalized exciton states.[18] The lack of cross peaks in the anisotropic 2D IR signal was attributed to the hydrogen disorder in ice I*h*, lifting any correlations between orientations of transition-dipole moments. Finally, we determined in Ref. 20 the vibrational lifetime in ice I*h*, which is very short compared to "normal" vibrations ($\lesssim$100 fs), as well as the time it takes to randomize the initial excitation energy, also very fast and on a similar time scale.

It should be added that the 2D IR spectra of neat ices have a very unconventional appearance[17,21] due to the multitude of possible coupling mechanisms (exciton coupling, exciton-phonon coupling, Fermi-resonance, and large anharmonicity) and are much harder to interpret than those of essentially monomeric molecular systems, such as metal-carbonyls that have been study extensively to establish 2D IR spectroscopy.[33] In this sense, the 2D IR spectroscopy of ice pushes the current boundaries of our ability to interpret 2D IR data. A general account of 2D IR spectroscopy is given in Ref. 34.

In the present paper, we extend the 2D IR work on ice I*h* towards high-pressure forms of ice. Thereby, we explore the structural variability that the polymorphism of ice offers and study its effect on the 2D IR spectroscopy. Ice II, ice V, and ice XIII have been chosen for this purpose, since this selection covers many aspects of all possible ice phases. To that end, a new preparation method had to be developed in order to obtain ultrathin films of these ices with good optical quality in a way that is compatible with transmission 2D IR spectroscopy. While at a first sight the 2D IR spectra of all ice phases look qualitatively similar, we will show that one can indeed distill out measures from experimental 2D IR spectra, which differentiate the various phases and which can be reproduced from simulated 2D IR spectra in a semi-quantitative manner and thus support a microscopic discussion of the coupling mechanisms.

A. Background: Ices I*h*, II, V, and XIII

The "ordinary" hexagonal ice I*h* occurs in vast quantities on our planet. Its wurtzite crystal structure with $P6_3/mmc$ space group symmetry consists of six-membered rings of hydrogen-bonded water molecules and displays characteristic open channels along the *c*-axis as shown in Fig. 1(c).[12,35] The unit cell of ice I*h* contains four fully hydrogen-disordered water molecules and two crystallographically distinct hydrogen-bonded O···O

distances which are almost identical in length. The O···O···O angles are in very close agreement with the tetrahedral angle.

Ice II was discovered by Tammann[36,37] and is thought to occur naturally on some of our solar system's icy moons.[38,39] It forms upon compression of ice I*h* below 238 K at ∼0.2 GPa, and its region of thermodynamic stability is separated from the liquid phase by other high-pressure phases.[40,41] Ice II is a fully hydrogen-ordered form of ice with $R\bar{3}$ space group symmetry.[42–44] It is the only phase of ice for which the hydrogen-disordered counterpart is unknown;[45] upon heating, it transforms to either ice I*h*, III, V, or VI depending on the pressure. Ice II has a hexagonal unit cell comprising 36 water molecules and four distinct types of hydrogen bonds of equal multiplicity.[42,43] The main structural feature is six-membered rings that form open channels along the crystallographic *c*-axis as can be seen in Fig. 1(d). These channels are interconnected with eight- and ten-membered rings.[3] In contrast to ice I*h*, the local hydrogen-bonding environment of ice II is distorted away from an ideal tetrahedral geometry. The root-mean-square deviation of the O···O···O angles from the tetrahedral angle is 16.8°.[43]

Ice V was discovered by Bridgman in the 0.3–0.6 GPa pressure range[40] and it displays the most complicated crystal structure of all the ice phases.[47] Its monoclinic unit cell with *A*2/*a* space group symmetry is shown in Fig. 1(e). It contains 28 water molecules, forming 4, 5, 6, 8, 9, 10, and 12-membered rings, and 8 crystallographically distinct hydrogen-bonded O···O distances.[47] Unlike the fully hydrogen-disordered ice I*h*, ice V displays partial hydrogen order with the fractional occupancies of some of the hydrogen positions deviating as much as 0.32 from $\frac{1}{2}$.[48] The distortions away from a tetrahedral local environment are even more pronounced in ice V than in ice II. The root-mean-square deviation of the O···O···O angles from the tetrahedral angle is 18.5°.[47,48]

The hydrogen-ordered counterpart of ice V, ice XIII with essentially the same oxygen structure and hydrogen-bonded network, forms upon cooling ice V doped with hydrochloric acid.[46] The acid dopant introduces mobile point defects which speed up molecular reorientation processes and therefore facilitate hydrogen ordering.[46,49–52] The ice V → ice XIII phase transition takes place upon isobaric cooling of ice V from its region of stability, but it can also be observed in a reversible fashion upon heating/cooling at ambient pressure with a phase transition temperature of 112 K.[50] Upon hydrogen-ordering, the space group changes from *A*2/*a* to $P2_1/a$, which is why also the oxygen structure changes slightly.[46] This leads to 7 crystallographically distinct water molecules and 14 different types of hydrogen bonds of equal multiplicity. Upon slow-cooling at ambient pressure, essentially fully hydrogen-ordered ice XIII samples can be obtained.[46,50] The spectroscopic differences between ice V and ice XIII have been investigated with Raman spectroscopy.[49]

II. METHODS

A. Preparation of thin films of high-pressure ices

Vibrational spectroscopy of high-pressure phases of ice often relies on Raman spectroscopy[16,49,53–62] which is straight-forward to perform using highly scattering powder samples. IR absorption spectra of some of the high-pressure phases of ice (i.e., ices II, IX, V, and VI) have also been recorded, again for polycrystalline powders, which had been mixed with an refractive-index-matching liquid at low temperatures to reduce the effects of light scattering.[63–65] Initial attempts to apply such mulling techniques to 2D IR spectroscopy in our lab failed, however, due to the large absorption background of the refractive-index-matching liquid and the still significant light scattering. The tested mulling liquids included isopentane, methane, ethane, propane, propylene, and mixtures thereof. In particular in the spectral range of the absorption bands of the ice, refractive-index matching is in fact very difficult, since the strong absorption bands of ice also affect its refractive index according to the Kramers-Kronig relationship.

Due to these difficulties, a different approach was taken here to prepare thin films of high-pressure phases of ice for 2D IR spectroscopy. The thickness of the films had to be within ∼1–2 μm, owing to the large absorption of the D_2O stretch band and the fact that the experiments had to be performed in transmission geometry. Since contamination of the samples with H_2O ice I*h* from moisture in the air is generally difficult to prevent, we focussed on preparing D_2O ices. To that end, D_2O was first degassed with three cycles of freeze-pump-thawing to remove CO_2 gas from D_2O. A thin film of liquid D_2O was then prepared between two circular *c*-cut sapphire windows of 10 mm diameter and 1 mm thickness. For this, a small drop of the D_2O was pipetted onto one of the discs and a second disc was firmly pressed against the first one while carefully preventing the formation of air bubbles. The perimeter of the "sandwiched" assembly was wrapped with a small strip of indium foil to stabilize the two windows and to prevent them from shearing against each other. In order to protect the outer window surfaces from condensation of water vapor, Teflon (PTFE) discs were attached with small strips of indium. The sample cell was then transferred into a 1.3 cm diameter stainless-steel pressure die from Specac, where it was cushioned from both sides with layers of graphite flakes. The pressure die was then sealed with stainless-steel pellets from the top and the bottom. A sketch of the entire assembly is shown in Fig. 2.

In a next step, the pressure die was fitted with a K-type thermocouple and submerged in liquid nitrogen which led to freezing of the thin water film inside the pressure die to give ice I*h*. Once liquid nitrogen temperature had been reached, pressure was applied onto the piston with a hand-operated 15 t hydraulic press. After removing the liquid nitrogen with a membrane pump, the sample was allowed to warm up under pressure. To prepare ice II, the pressure die was heated at 0.4 GPa to 235 K. For the ice V/XIII sample, 10 mM DCl was added to the initial sample solution and the sample was heated at 0.6 GPa to 250 K.[46] Once the target phase of ice had been formed under pressure, the pressure die was cooled back to liquid nitrogen temperature. The pressure then could be release. The pressures displayed by the hydraulic press were calibrated by measuring the melting points of larger ice samples under pressure and comparison with literature values.[66]

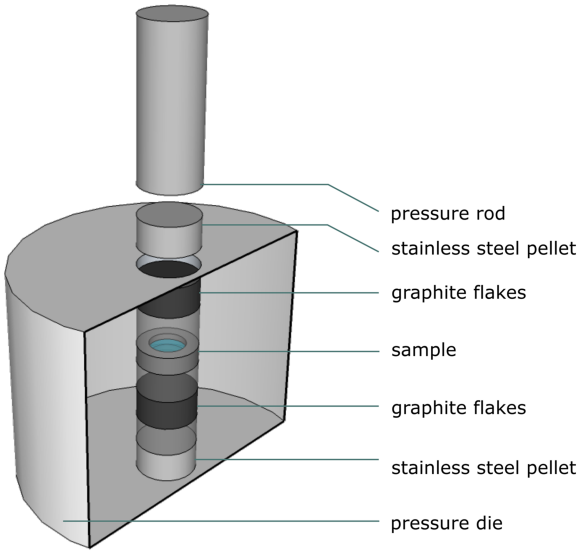

FIG. 2. Cutaway schematic of the stacking inside the pressure die. Sapphire windows inside the core of the die encase the ice sample and are wrapped with a small strip of indium foil. Graphite flakes prevent the windows from touching the walls of the cavity. Fitted stainless steel pellets seal the openings. The pressure is applied with a hand operated hydraulic press from the top with a pressure rod.

The sample cell containing the high-pressure ices was retrieved from the pressure die under liquid nitrogen, cleaned from the graphite, and the PTFE discs were removed. The window assembly was then transferred into a pre-cooled, purpose-made cryostat under liquid nitrogen, and the cryostat was finally closed and evacuated. Small amounts of H_2O ice I*h* condensed on the window surfaces during the short period of time when the sample cell was exposed to open air (~3 s). This turned out to be the dominating source of light scattering in the 2D IR experiments.

In the case of the ice II samples, residual CO_2 was removed by heating the sample to 140 K for 5 min inside the cryostat. The actual IR experiments were then performed at ~80 K. The preparation of ice XIII samples required an additional heating/cooling step inside the cryostat.[49,50] The initial sample retrieved from the pressure die resembled ice V since it was cooled quickly under pressure.[50] The phase transformation to ice XIII was achieved by heating to 135 K and subsequent slow-cooling to 90 K at 0.1 K min^{-1}. Ice XIII was then measured at ~80 K. The same sample could also be used to measure ice V after reheating to 135 K. The complete removal of CO_2 was observed during the first slow-cooling step. Standard FTIR linear absorption spectra were recorded in transmission geometry using a FTIR spectrometer (Tensor 27 by Bruker) with the slit opening reduced to 0.5 mm to act as a pinhole to reduce scattering.

B. 2D IR spectroscopy

The setup for recording 2D IR spectra was similar to that previously described.[67] In brief, the output of a Ti:S amplified laser system (repetition rate 1 kHz) feed an optical parametric amplifier (OPA), which generated tunable broadband femtosecond mid-IR pulses centered around the OD-stretch vibration of ice at 2375 cm^{-1} with an energy of ~2 μJ.[68] A 2D IR spectroscopy setup in pump-probe geometry with an interferometer in the pump arm as described in Ref. 67 was used. The coherence time was scanned between (−500, 1500) fs, resulting in a resolution of 11 cm^{-1}/pixel in the pump-frequency dimension after zero-padding by a factor 2.[34] The transmitted probe beam was dispersed in a monochromator and detected by a double-array HgCdTe (MCT) detector with 32 pixels for frequency-resolved detection with a spectral resolution of 15 cm^{-1}/pixel in the probe frequency dimension. 2D IR spectra were recorded for population times varied from 150 fs to 1 ps.

Polarization-control was achieved with an automatized λ/2-waveplate that flipped the pump-pulse polarization between successive scans. Data were taken in the S_{ZZZZ} and the S_{YYZZ} polarization geometry (with S_{ZZZZ} being the signal with all field interactions polarized in parallel in the z-direction and S_{YYZZ} that with pump- and probe-process being polarized perpendicularly), from which the isotropic [$S_{iso} = (S_{ZZZZ} + 2S_{YYZZ})/3$] and anisotropic ($S_{aniso} = S_{ZZZZ} - S_{YYZZ}$) 2D IR spectra were calculated.

Scattering of the sample turned out to be a major issue, and in order to suppress it, several measures were employed in concert. First, trivially, pinholes were used to block scattered light as much as possible. Second, a wobbling Brewster window was introduced in the pump beam, running at 1/4 of the laser repetition rate and generating a (π, 0, $-\pi$, 0) quasi-phase sequence,[67,69] in order to eliminate the interference of probe-light with scattered pump-light. Higher order terms were reduced by additional population time modulation.[67] Third, pump-pump-scattering was suppressed with the help of a shutter that blocks the probe-light during every other scan and by subtracting that background measurement from the signal. Finally, 2D IR spectra measured at negative population times were subtracted in order to eliminate also the incoherent contribution to scattering.

From the absorbed pulse energy, measurement volume, and heat capacity, we estimated that the measurement spot heats by 1.5 K per shot. The ice layer is very thin (~1–2 μm) and the heat conductivity of the window material sapphire is quite large, so we can safely assume that heat does not accumulate but dissipates into the window until the subsequent laser shot. We did not observe any phase transition induced by the laser.

C. Spectral simulations

Molecular dynamics simulations were performed using the GROMACS 4.6.1 suite.[70] The starting structure for the ordered phase of ice II was generated from the crystallographic structure,[42,43] and the unit cell was replicated in the x, y, and z directions giving rise to a rhombohedral $4 \times 3 \times 3$ supercell of dimensions $3.1 \times 2.3 \times 2.3$ nm containing 432 water molecules and a total of 864 OD-stretch vibrations. The water molecules were described using the Simple Point Charge-Extended (SPC/E) model.[71] The Lennard-Jones (LJ) and the Coulomb interactions were truncated at 0.9 nm, in which a cutoff scheme was used for the LJ interactions, and the Particle-Mesh-Ewald (PME) summation scheme[72] for the Coulomb ones. The bonds were constrained using the LINCS algorithm.[73] The structure was equilibrated for 1 ns at constant pressure (1 bar) and temperature (80 K). The pressure

was maintained constant using an anisotropic pressure coupling[74] with a Parrinello-Rahman barostat (τ_P = 2.0 ps).[75] A V-rescale thermostat was used to maintain the temperature constant (τ_T = 0.2 ps).[76] The time step in all simulations was 1.0 fs. Using the equilibrium density, a constant volume production run at 80 K with a length of 200 ps was performed. The atomic positions were stored at each 5 fs for the spectral calculations.

The OD-stretch vibrations were modelled using a time-dependent Hamiltonian of the following form:

$$H(t) = \sum_i \omega_i(t) B_i^\dagger B_i - \frac{\Delta}{2} \sum_i B_i^\dagger B_i^\dagger B_i B_i + \sum_{i,j} J_{ij}(t) B_i^\dagger B_j - \sum_i \vec{\mu_i}(t) \cdot \vec{E}(t)(B_i^\dagger + B_i), \quad (1)$$

where $B_i^\dagger$ and B_i are the Bosonic creation and annihilation operators and ω_i and μ_i are the site frequencies and the site transition dipole moment, respectively. $\vec{E}(t)$ is the applied laser field. The anharmonicity Δ was fixed at 200 cm^{-1}. The frequency for each local OD-stretch vibration was determined using an electrostatic frequency map[22,77,78] relating the this frequency to the electric field E_i^{OD} (given in $E_h e/a_0$) exerted by the other water molecules on the involved deuterium atom in the direction of the OD-bond,

$$\omega_i = 2802.2 - 2572.2 \cdot E_i^{OD} - 1.0298 \times 10^5 (E_i^{OD})^2, \quad (2)$$

where the frequencies are given in units of wavenumbers. The frequency offset, 2802.2 cm^{-1}, was adjusted to roughly match the experimental spectrum. This offset is somewhat arbitrary, as the electric field of the water model is not exact.[79]

The intramolecular couplings between the water OD stretches were calculated using a mechanical coupling model,[78]

$$J_{ij} = (-1789 + 23852(E_i^{OD} + E_j^{OD}))x_i x_j - 1.996 p_i p_j. \quad (3)$$

Here the amplitude and momentum parameters are (in atomic units)[77]

$$x_i = 0.1024 - 0.927 \times 10^{-5} \omega_{OD}, \quad p_i = 1.6466 + 5.7697 \times 10^{-4} \omega_{OD}. \quad (4)$$

The intermolecular coupling is given by the transition dipole coupling model,[22]

$$J_{ij} = A \frac{\mu_i' \mu_j' (\hat{u}_i \cdot \hat{u}_j - 3(\hat{u}_i \cdot \hat{n}_{ij})(\hat{u}_j \cdot \hat{n}_{ij}))}{r_{ij}^3}. \quad (5)$$

The transition dipoles were located on the OD-bond and assumed to be parallel with the bond.[77] r_{ij} is the distance between these for different OD-bonds on different water molecules, and $\hat{n}_{ij}$ is the unit vector connecting the transition dipoles. A is a conversion factor between the involved units, with A = 32.8 cm^{-1}nm$^3 a_0^{-2} e^{-2}$. The transition dipole moment of each local mode is[78]

$$\mu_i' = 0.1622 + 10.381 E_i^{OD} + 137.6 (E_i^{OD})^2, \quad \vec{\mu}_i = x_i \cdot \mu_i' \hat{u}_i. \quad (6)$$

Here $\hat{u}_i$ is a unit vector along the OD bond. The distance between the transition dipoles is very short for hydrogen bonded water molecules and one can imagine multipole effects playing a role. This may be reflected in the scatter found in the fits correlating couplings found through density functional theory (DFT) calculations and the model when optimizing the position along the bond.[77] Still, calculations using this coupling model have given very good results in the past.[77]

The spectra were calculated using the Numerical Integration of Schrödinger Equation (NISE) method,[80] with coherence times varied from 0 to 1500 fs and an *ad hoc* lifetime of 700 fs applied during the coherence times for spectral apodization. The 2D IR spectra were obtained by sampling at 10 ps intervals along the 200 ps trajectory resulting in a total of 20 realizations. The absorption spectra were obtained by sampling at 100 fs intervals resulting in 1970 realizations.

III. RESULTS AND DISCUSSION

A. IR absorption spectra

Figure 3(b) (red line) shows the absorption spectrum of neat ice II. The spectrum shows three main peaks at 2395 cm^{-1}, 2427 cm^{-1}, and 2528 cm^{-1} together with smaller shoulders at 2474 cm^{-1} and 2505 cm^{-1}. The signal-to-noise ratio of the spectrum is much better than that reported by Bertie and Whalley,[64] but otherwise agrees with it reasonably well. That older spectrum was measured using a mulling technique together with a refractive index matching liquid, and we consider the good agreement of both spectra a verification of the reliability of our preparation technique (see Sec. II).

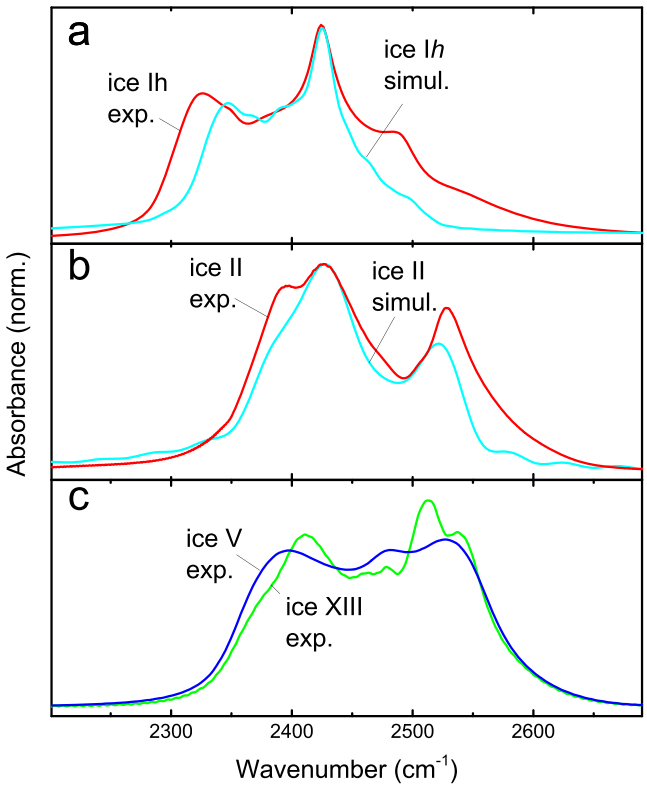

FIG. 3. (a) The experimental and simulated absorption spectra of D_2O ice I*h* at ~80 K are shown in red and cyan, respectively, (b) same for neat D_2O ice II at ~80 K, and (c) experimental absorption spectra of neat D_2O ice V at ~135 K (blue) and ice XIII at ~80 K (green). (a) Reproduced with permission from L. Shi *et al.*, Phys. Chem. Chem. Phys. **18**, 3772 (2016). Copyright 2016 Royal Society of Chemistry.

Shown in Fig. 3(a) is the absorption spectrum of ice I*h* (red line) for comparison. Overall speaking, the ice II absorption spectrum is blue-shifted relative to ice I*h*, indicating weaker hydrogen bonds in ice II despite its higher density. This is a general observation for all high-pressure forms of ice and reflects the increased distances to neighbouring hydrogen-bonded water molecules as the water molecules are packed more efficiently, the so-called pressure-distance paradox. Somewhat surprisingly, however, the widths of the various spectral features in ice II and ice I*h* are very much comparable, despite the fact that ice II is hydrogen-ordered and ice I*h* is hydrogen-disordered.

Just like for ice I*h* [shown in Fig. 3(a), cyan line],[21] the spectrum of ice II can almost quantitatively be reproduced by the spectral simulations with regard to the band structure as well as the width of the absorption peaks, see Fig. 3(b) (cyan line). The peak on the red side of the spectrum is less pronounced in theory than in experiment. This discrepancy reflects the relative intensity of the peaks, which is determined by a combination of the coupling and the direction of the transition dipoles. The relative peak positions, on the other hand, are determined by the couplings and these are reproduced quite accurately, suggesting that the slight difference in peak intensities is rather due to a minor mismatch in the directions of the site transition dipoles, which in the model are assumed to be along the OD-bonds. The transition dipoles of states comprising the low-frequency peak and shoulder are predominantly in the hexagonal (*a*, *b*)-plane corresponding to E_u symmetry, while the transition dipoles connected with high frequency peak are in the direction of the hexagonal *c*-axis corresponding to A_u symmetry. This symmetry of the vibrational modes is partially broken due to thermal fluctuations.

Figure 3(c) compares the absorption spectra of neat ice V (blue) and ice XIII at 150 K (green). The spectrum of the hydrogen-disordered ice V, which is consistent with a spectrum reported by Bertie and Whalley,[64] is less resolved with three discernable peaks at 2400 cm^{-1}, 2484 cm^{-1}, and 2525 cm^{-1}. These spectral features evolve additional substructure in the hydrogen-ordered form ice XIII with resolved peaks at 2374 cm^{-1}, 2410 cm^{-1}, 2460 cm^{-1}, 2478 cm^{-1}, 2513 cm^{-1}, and 2537 cm^{-1}. Ice XIII is more congested than the also hydrogen-ordered ice II, reflecting the more complex crystal structure with 28 IR-active OD-stretching modes instead of 12.

Using the same approach as for ice I*h*[21] and ice II, we were however not able to reproduce the absorption spectra of ice V and ice XIII by the spectral simulations in a qualitatively correct way; the obtained spectra were significantly too broad and largely smeared out. This can be attributed to the complex and highly strained structures of ices V/XIII, strongly deviating from a locally tetrahedral structure (by 18.5°[47,48]), which may not be described well by the SPC/E model that was developed for liquid water dominated by tetrahedral hydrogen-bond environments. That is, in the MD simulation, the local structures may deviate from the real ice structure, thereby introducing an additional structural source of inhomogeneity. In fact, it has been shown that high-level computational recipes including descriptions of van der Waals interactions are required for a reliable computational treatment of ices V/XIII.[81]

B. 2D IR spectra of ice II

Figures 4 and 5(a) present time-series of the experimental 2D IR spectra of ice I*h* (reproduced from Refs. 20 and 21 and shown here for comparison) and ice II, respectively, in either case, both the isotropic [$S_{iso} = (S_{ZZZZ} + 2S_{YYZZ})/3$] and the anisotropic ($S_{aniso} = S_{ZZZZ} - S_{YYZZ}$) spectra. The reasoning for doing that is the following: The isotropic spectrum, which averages over all orientations, does not decay to zero since lattice heating after vibrational relaxation leads to an additional, difficult to interpret 2D IR response. In order to suppress that thermal signal, we therefore also plot the anisotropic spectrum, which does indeed decay to zero as the excitation energy looses the memory on the orientation of the originally pumped transition dipole.

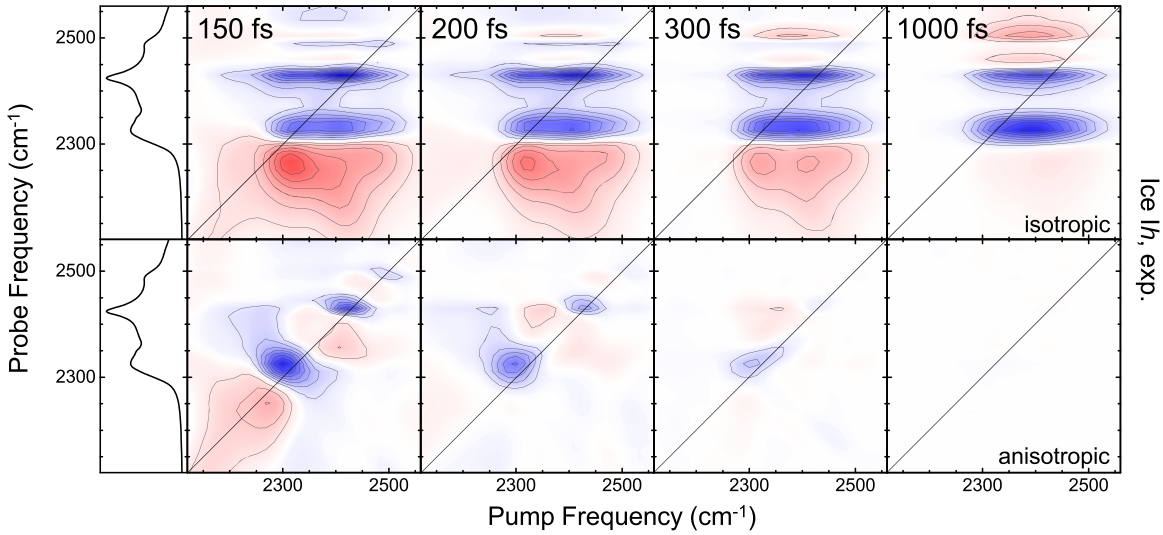

FIG. 4. Experimental 2D IR spectra of neat D_2O ice I*h*. The top row shows the isotropic 2D IR spectra $S_{iso} = (S_{ZZZZ} + 2S_{YYZZ})/3$ at population times varied from 150 fs to 1000 fs and the bottom row the corresponding anisotropic 2D IR spectra $S_{aniso} = S_{ZZZZ} - S_{YYZZ}$. The left-most panels show the absorption spectra from Fig. 3(a) for comparison. Blue and red features correspond to the 0–1 and 1–2 transitions, respectively. The data are reproduced from Ref. 20 with permission from the Royal Society of Chemistry and are shown here for better comparison with the other ice phases.

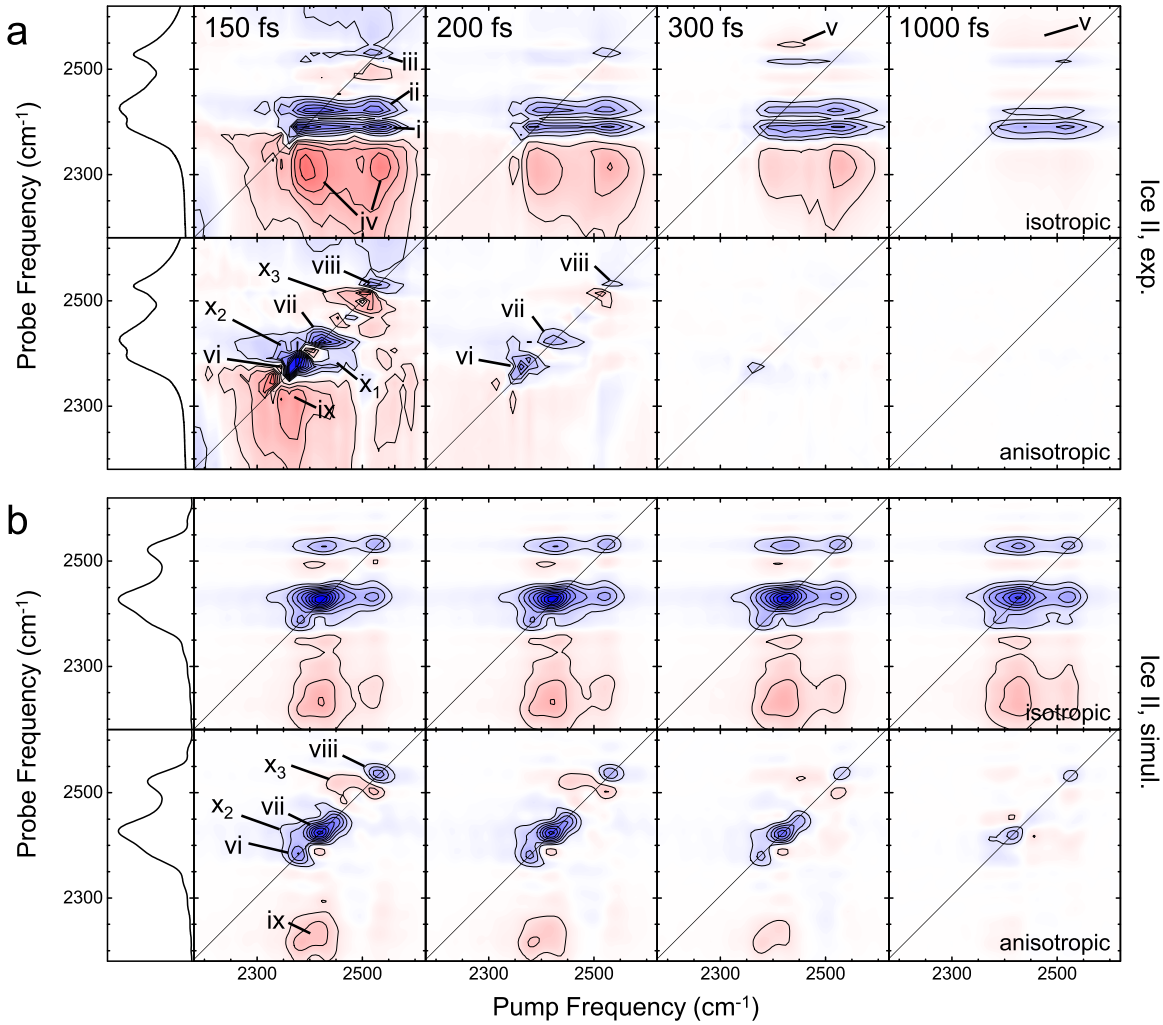

FIG. 5. Experimental (a) and simulated (b) 2D IR spectra of neat D_2O ice II at ~80 K. In either case, the top row shows the isotropic 2D IR spectra $S_{iso} = (S_{ZZZZ} + 2S_{YYZZ})/3$ at population times varied from 150 fs to 1000 fs and the bottom row shows the corresponding anisotropic 2D IR spectra $S_{aniso} = S_{ZZZZ} - S_{YYZZ}$. Labeled bands are discussed in the text. The left-most panels show the absorption spectra from Fig. 3(b) for comparison. Blue and red features correspond to the 0–1 and 1–2 transitions, respectively.

Overall, the 2D IR spectra of ice II [Fig. 5(a)] are very similar to those of ice I*h* (Fig. 4), apart from the already discussed frequency blueshift resulting from the weaker hydrogen bonds in ice II. That is, the isotropic 2D IR spectrum at population time 150 fs exhibits three elongated peaks from the ground state bleach [bands labeled as i-iii in Fig. 5(a), shown in blue] that match the frequencies of the bands in the absorption spectrum (left-most panel). In the common language of 2D IR spectroscopy, these bands would be assigned to the 0–1 transitions between ground and first excited states.[34] Their elongation along the pump-frequency axis can be understood as merging cross peaks due to strong excitonic coupling. The cross peaks lead to horizontal features along the pump-frequency axis, which is related to the interference between bleach peaks and weaker 1–2 excited state absorption peaks, that is, the spectra are more congested along the probe direction than along the pump direction, leading to these distorted peak shapes. The lowest-frequency excited state absorption bands, on the other hand, are spectrally isolated (bands iv shown in red) and appear in similar fashion also in the 2D IR spectra of neat ice I*h*[20] and isotope diluted ice I*h*.[17] They are much broader than the corresponding bleach signal (band i), an effect that has been attributed to the coupling of the OD stretch vibration to lattice phonons that is stronger in the excited state due to the large anharmonicity of the OD-potential.[17]

Another red band (band v) emerges on the opposite side of the spectrum at later population times (≳300 fs). A similar response is found in 2D IR spectra and pump-probe spectra of ice I*h*[17,20,82,83] and liquid water,[84,85] and has been attributed to weakening of the hydrogen bonds upon heating of the lattice after vibrational relaxation, causing a general blueshift of the OD stretch vibration.

The anisotropic spectrum is dominated by on-diagonal peaks that correspond to the main peaks of the absorption spectrum, again very similar to ice I*h*. These peaks exhibit different line shapes, as can be seen in the 150 fs spectrum, and even better in the 200 fs spectrum, which is less crowded. That is, the lowest frequency band vi is slightly elongated along the diagonal, indicating some degree of inhomogeneous broadening despite the fact that it is a hydrogen-ordered form of ice. On the other hand, bands vii and viii are elongated along the

pump-frequency axis instead with basically no evidence for inhomogeneous broadening. Bands x_1 and x_2 in the 150 fs spectrum indicate cross peaks between bands vi and vii, and band x_3 indicates a cross peak between bands vii and viii with an opposite sign.

In Fig. 5(b), we show the corresponding 2D IR spectra from the spectral simulations. The isotropic spectra [Fig. 5(b), first row] are dominated by multiple bleach peaks. In good agreement with the experimental results, the positions of these peaks correspond to the two main transitions and the low frequency shoulder in the IR absorption spectra (left-most panel). The low-frequency shoulder is weaker in the simulation, as was already discussed for the IR absorption spectrum. The peaks are interfering with exited state absorption peaks, which results in peak shapes squeezed in the probe frequency direction. No significant signature of peak shape dynamics is observable, similarly to the observations for ice I*h*.[21] This is a result of the strong exchange narrowing observed in both ices due to the large vibrational couplings. As a result of the coupling, the frequencies of the eigenstates are effectively averaged over the local mode frequencies and fluctuations are washed out making it difficult to discern any spectral dynamics. Furthermore, the lineshapes are affected by interference between bleach and absorption features making extraction of spectral dynamics even more difficult.

The anisotropic spectra [Fig. 5(b), second row] obtained from the simulations are characterized by three diagonal bleach peaks vi, vii, and viii. These correspond well with the peaks found in the IR absorption spectrum and again the simulated spectra correspond well with the experimental ones. However, the simulated peaks are generally narrower than the experimental ones, which may be related to lifetime broadening. As in the IR absorption spectrum, the relative intensity of the different peaks is not perfectly matching the experiment. Furthermore, the simulated excited state absorption peaks (band ix) appear to be slightly too weak in the simulated 2D IR spectra.

As already discussed for the linear absorption spectra, we found that the states giving rise to the vi and vii peaks have E_u-symmetry and, thus, consists of degenerate pairs of states with transition dipoles in the hexagonal (a, b)-plane. The viii peak is formed by non-degenerate states with A_u-symmetry and transition dipoles along the hexagonal c-axis. Disorder in hydrogen bond strength breaks the degeneracy of the E_u-symmetry, leading to higher inhomogeneity in the vi and vii peaks than in the viii peak with A_u-symmetry. It may still appear quite surprising that peaks in the ice II spectrum are inhomogeneously broadened, while the peaks in the corresponding ice I*h* spectrum are not. The peak in the Raman spectrum of isotope diluted ice I*h* is broader[86] than the width of the corresponding peaks in ice II.[61] However, in isotope diluted ice I*h* the width of the single peak arise from two essentially identical hydrogen bonding environments, while in isotope diluted ice II four clearly distinguishable peaks arising from four distinct hydrogen bond types are present in the spectra. The distance between the lowest and highest-frequency peaks is about 50 cm^{-1}, which is comparable to the couplings between the OD-stretch vibrations in neat ice II. The vibrations in neat ice II are, thus, delocalized over local vibrations with different hydrogen bond environments and the inhomogeneity is picked up from the spread in local mode frequencies.

The positive cross peak in the anisotropic 2D IR spectrum at the x_2 position observed both in experiment and theory suggests orientational correlation of the vibrations involved. The ratio between the anisotropic and isotropic signals at this position is about 0.1, which is in agreement with a cross peak between pairs of states that have the transition dipoles randomly distributed within the same fixed plane. In this case, this plane is the hexagonal plane of the ice II lattice. At the above diagonal cross peak position x_3 between the vii and viii bands, the anisotropic signal in both theory and experiment is weak but negative. The ratio between the anisotropic and isotropic signals is about −0.1, which is consistent with a cross peak between pairs of states with transition dipoles that are perpendicular to each other. This is in line with the symmetry assignment of the involved vibrations. Cross peaks may be present below the diagonal as well; however, these are difficult to assign due to interference with excited state absorption peaks.

C. 2D IR spectra of ice V and ice XIII

Somewhat surprisingly, the differences of the experimental 2D IR spectra of ice V [Fig. 6(a)] and ice XIII [Fig. 6(b)] are significantly more pronounced than those of ice I*h* and ice II. Both couples, ice V/ice XIII and ice I*h*/ice II, are hydrogen-disordered vs. hydrogen-ordered forms of ice, respectively, but in contrast to ice I*h*/ice II, ice V and ice XIII share essentially the same oxygen structure. For the most part, the differences in the 2D IR spectra of ice V and ice XIII reflect what has already been seen in the IR absorption spectra [Fig. 3(c)]. That is, the more structured absorption spectrum of hydrogen-ordered ice XIII results in more structured 2D IR spectra, both the isotropic and the anisotropic ones. Independent of that, we find that band xi in the anisotropic 2D IR spectrum of ice V is clearly tilted along the diagonal, in contrast to the corresponding band in ice XIII. This difference is expected since hydrogen-disorder induces a certain degree of static inhomogenous broadening. However, it is again only the lowest-frequency band for which such a tilt along the diagonal is observed, similar to band vi in ice II [Fig. 5(a)].

As in the case of ice I*h* and ice II, the isotropic 2D IR spectra of ice V and ice XIII do not decay to zero at longer population time, since lattice heating after vibrational relaxation weakens the hydrogen bonds that result in a general blueshift of the absorption spectrum. On the other hand, the anisotropic 2D IR spectrum decays very quickly due to vibrational relaxation and the randomization of the excitation. For the ice XIII spectra, a number of cross peaks are observed above the diagonal. In particular, the negative cross peak x suggests that the transition dipoles of corresponding vibrational states are close to perpendicular to each other. Similar cross peaks are absent in the ice V spectrum, indicating that the orientational order giving rise to the cross peaks in ice XIII is lacking here.

As we were not able to reproduce IR absorption spectra of ice V and ice XIII in a qualitatively correct way with

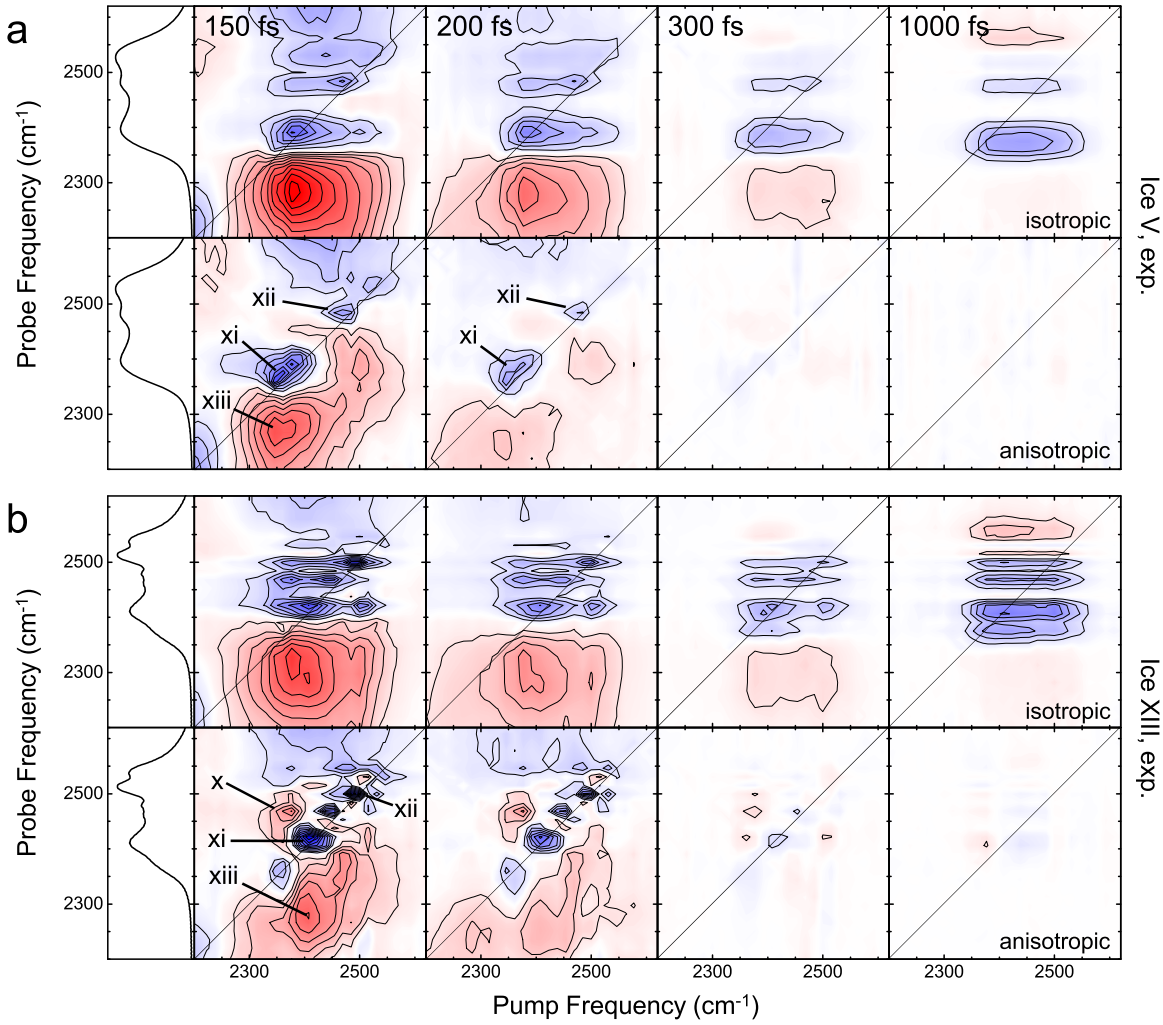

FIG. 6. Experimental 2D IR spectra of (a) neat D_2O ice V at ~80 K and (b) ice XIII at 135 K. The top row shows the isotropic 2D IR spectra $S_{iso} = (S_{ZZZZ} + 2S_{YYZZ})/3$ at population times varied from 150 fs to 1000 fs and the bottom row shows the corresponding anisotropic 2D IR spectra $S_{aniso} = S_{ZZZZ} - S_{YYZZ}$. Labeled bands are discussed in the text. The left-most panels show the 1D absorption spectra from Fig. 3(c) for comparison. Blue and red features correspond to the 0–1 and 1–2 transitions, respectively.

our simulation protocol, we did not attempt to simulate the corresponding 2D IR spectra.

D. Exciton migration

Figure 7 shows the decay of the anisotropic 2D IR spectra as a function of population time. The anisotropic 2D IR spectra decay much faster than the isotropic 2D IR spectra, both in the experiment and in the simulation (Figs. 5 and 6). The decay of the anisotropic 2D IR spectra reflects the loss of memory of the orientation of the initially pumped transition dipole. Two effects contribute to that loss of memory: vibrational relaxation leading to a heating of the crystal and a general blueshift of all vibrational modes, irrespective of their transition dipole direction, as well as exciton-migration. The experimentally obtained anisotropy decay is essentially the same for all ices, including ice I*h* [for the latter, see Fig. 4(b) of Ref. 20], regardless of whether it is a hydrogen-ordered or hydrogen-disordered form of ice, even though the presence of cross peaks may hint at the presence of hydrogen order through correlation of the transition dipole directions.

The agreement with the results from the spectral simulation is rather modest [compare Fig. 7(a) vs. Fig. 7(b)]. That is, diagonal peaks in the anisotropic spectra decay significantly slower and are still partially present even at 1 ps population time in the simulated spectrum, whereas in the experiment these are essentially gone at 300 fs. This is consistent with what has been reported for ice I*h*[21] and is likely resulting from the neglect of relaxation out of the OD-stretch manifold in the simulations. The inclusion of relaxation would be computationally too demanding for a large system such as ice.[87–90] This also implies that the thermal signal expected to appear after heating due to energy transferred from the OD-vibrations to low frequency vibrations of the lattice is not included either. The thermal signal is expected to be isotropic in nature, dominating the experimental isotropic signal at 1 ps. As previously stated in Ref. 21, this complicates the interpretation of the isotropic signal, since the origin is difficult to determine without theoretical support. The partial (slow) decay of the diagonal peaks, on the other hand, reflects the loss of orientation upon exciton migration.

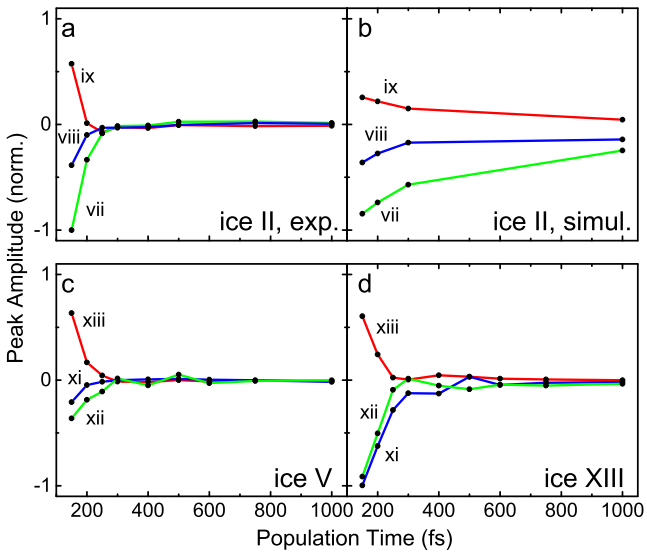

FIG. 7. Time-dependence of various peaks in the anisotropic 2D IR spectra as labeled in Fig. 5. (a) shows the experimental results for ice II, (b) shows the simulation results of ice II, and (c) and (d) show the experimental results of ice V and ice XIII, respectively.

IV. CONCLUSION

In conclusion, we have presented experimental and simulated 2D IR spectra of some high-pressure forms of isotope-pure D_2O ice, i.e., of ice II, ice V, and ice XIII, thereby extending our previous work on ice I*h*.[20,21] We explore to what extent the structural variability, which the polymorphism of ice offers, is reflected in the 2D IR spectroscopy. 2D IR spectra of all investigated forms of ice are quite unconventional and differ significantly from those of molecular systems.[34] On the one hand, this is caused by the large exciton coupling that strongly delocalizes the first excited states. On the other hand, the anharmonicity of the OD-bond is also very large [$\Delta = 200\ \mathrm{cm}^{-1}$, see Eq. (2)], hence the doubly excited states tend to localize again. Therefore, it is no longer possible to assign a 1–2 transition (depicted in red in Figs. 4–6) to each of the 0–1 transitions (depicted in blue), which for the most part is responsible for the unconventional appearance of the 2D IR spectra of ice. Nonetheless, since the simulation results reveal good qualitative agreement with the experimental spectra, we conclude that the Hamiltonian Eq. (2) fully captures the physics of these spectra. That Hamiltonian in essence is the standard Hamiltonian used for all applications of 2D IR spectroscopy,[34] also those of molecular systems with a more conventional appearance. The Hamiltonian includes exciton coupling and in a semi-classical sense also the coupling of the excitons to lattice phonons (external phonons). However, it ignores a possible Fermi-resonance with the DOD-bending modes of water, a mechanism that is sometimes made responsible for the complicated spectroscopy of water in its various states of aggregation as well. Fermi-resonances lead to specific pattern in the 2D IR spectra,[91] however, do not seem to play a significant role here as the experimental spectra are well reproduced without including these.

The hydrogen-ordered ice II appears to be more inhomogeneously broadened than the hydrogen-disordered ice I*h*, as manifested by a tilted 2D IR line, the equivalent of which has not been observed in ice I*h*.[20] This can be explained by the presence of four well-defined and distinct hydrogen-bond strengths in ice II leading to a static distribution of frequencies, which are scrambled in the delocalized states resulting from the exciton coupling. Ice V and ice XIII, on the other hand, behave as expected with the hydrogen-disordered case (ice V) being more inhomogenously broadened. Finally, the presence of above diagonal cross peaks in the anisotropic 2D IR spectra for the hydrogen-ordered ice II and ice XIII phases was explained by symmetry-imposed orientational correlations of the transition dipoles for the involved state pairs. In the corresponding spectra of ice I*h* and ice V, no such cross peak was observed. This suggests that such cross peaks can be seen as markers for hydrogen-order.

To wrap up, the rich peak structure observed in the 2D IR spectra of all forms of ice is caused by the complex interplay between static structural disorder resulting from inherently different hydrogen-bond conformations, excitonic couplings mixing these states in delocalized vibrations, thermal relaxation, and strong anharmonicities resulting in localization of the double excited states. This is further combined with the hydrogen-order or lack thereof. With the present analysis, we have extended the realm for which 2D IR spectra can be understood and structural insight can be deduced.

ACKNOWLEDGMENTS

We thank Jan Helbing for crucial help with the 2D IR setup, Stewart Clark for helpful discussions regarding the vibrational spectroscopy of ices, and Carlos Vega for helpful discussions and for sharing ice structures used to validate the employed MD starting structures. The work has been supported in part by the Swiss National Science Foundation (SNF) through the NCCR MUST to P.H., by the Royal Society International Exchanges Scheme Grant (No. IE131094) to C.G.S. and P.H., and by a Royal Society University Research Fellowship (No. UF150665) as well as a Leverhulme Research Grant (No. RPG-2014-04) to C.G.S.

[1] P. Ball, Nature **452**, 291 (2008).
[2] P. Gallo, K. Amann-Winkel, C. A. Angell, M. A. Anisimov, F. Caupin, C. Chakravarty, E. Lascaris, T. Loerting, A. Z. Panagiotopoulos, J. Russo, J. A. Sellberg, H. E. Stanley, H. Tanaka, C. Vega, L. Xu, and L. G. M. Pettersson, Chem. Rev. **116**, 7463 (2016).
[3] C. G. Salzmann, P. G. Radaelli, B. Slater, and J. L. Finney, Phys. Chem. Chem. Phys. **13**, 18468 (2011).
[4] A. Falenty, T. C. Hansen, and W. F. Kuhs, Nature **516**, 231 (2014).
[5] L. del Rosso, M. Celli, and L. Ulivi, Nat. Commun. **7**, 13394 (2016).
[6] T. Loerting, K. Winkel, M. Seidl, M. Bauer, C. Mitterdorfer, P. H. Handle, C. G. Salzmann, E. Mayer, J. L. Finney, and D. T. Bowron, Phys. Chem. Chem. Phys. **13**, 8783 (2011).
[7] J. J. Shephard, J. S. O. Evans, and C. G. Salzmann, J. Phys. Chem. Lett. **4**, 3672 (2013).
[8] J. J. Shephard, S. Klotz, M. Vickers, and C. G. Salzmann, J. Chem. Phys. **144**, 204502 (2016).
[9] T. L. Malkin, B. J. Murray, A. V. Brukhno, J. Anwar, and C. G. Salzmann, Proc. Natl. Acad. Sci. U. S. A. **109**, 1041 (2012).
[10] W. F. Kuhs, C. Sippel, A. Falenty, and T. C. Hansen, Proc. Natl. Acad. Sci. U. S. A. **109**, 21259 (2012).
[11] T. L. Malkin, B. J. Murray, C. G. Salzmann, V. Molinero, S. J. Pickering, and T. F. Whale, Phys. Chem. Chem. Phys. **17**, 60 (2015).
[12] E. O. Wollan, W. L. Davidson, and C. G. Shull, Phys. Rev. **75**, 1348 (1949).
[13] G. L. Richmond, Chem. Rev. **102**, 2693 (2002).

[14]H. J. Bakker and J. L. Skinner, Chem. Rev. **110**, 1498 (2010).
[15]M. J. Shultz, T. H. Vu, B. Meyer, and P. Bisson, Acc. Chem. Res. **45**, 15 (2012).
[16]T. F. Whale, S. J. Clark, J. L. Finney, and C. G. Salzmann, J. Raman Spectrosc. **44**, 290 (2013).
[17]F. Perakis, S. Widmer, and P. Hamm, J. Chem. Phys. **134**, 204505 (2011).
[18]L. Shi and J. L. Skinner, J. Phys. Chem. B **117**, 15536 (2013).
[19]A. Shalit, F. Perakis, and P. Hamm, J. Chem. Phys. **140**, 151102 (2014).
[20]F. Perakis and P. Hamm, Phys. Chem. Chem. Phys. **14**, 6250 (2012).
[21]L. Shi, J. L. Skinner, and T. L. C. Jansen, Phys. Chem. Chem. Phys. **18**, 3772 (2016).
[22]F. Li and J. L. Skinner, J. Chem. Phys. **133**, 244504 (2010).
[23]L. Shi, S. M. Gruenbaum, and J. L. Skinner, J. Phys. Chem. B **116**, 13821 (2012).
[24]P. Hamm, M. H. Lim, and R. M. Hochstrasser, J. Chem. Phys. **107**, 10523 (1997).
[25]M. L. Cowan, B. D. Bruner, N. Huse, J. R. Dwyer, B. Chugh, E. T. J. Nibbering, T. Elsaesser, and R. J. D. Miller, Nature **434**, 199 (2005).
[26]L. De Marco, W. Carpenter, H. Liu, R. Biswas, J. M. Bowman, and A. Tokmakoff, J. Phys. Chem. Lett. **7**, 1769 (2016).
[27]R. McGraw, W. G. Madden, S. A. Rice, and M. G. Sceats, Chem. Phys. Lett. **48**, 219 (1977).
[28]J. Bredenbeck and P. Hamm, J. Chem. Phys. **119**, 1569 (2003).
[29]J. B. Asbury, T. Steinel, K. Kwak, S. A. Corcelli, C. P. Lawrence, J. L. Skinner, and M. D. Fayer, J. Chem. Phys. **121**, 12431 (2004).
[30]S. Yeremenko, M. S. Pshenichnikov, and D. A. Wiersma, Chem. Phys. Lett. **369**, 107 (2003).
[31]J. D. Eaves, J. J. Loparo, C. J. Fecko, S. T. Roberts, A. Tokmakoff, and P. L. Geissler, Proc. Natl. Acad. Sci. U. S. A. **102**, 13019 (2005).
[32]T. L. C. Jansen, B. M. Auer, M. Yang, and J. L. Skinner, J. Chem. Phys. **132**, 224503 (2010).
[33]O. Golonzka, M. Khalil, N. Demirdöven, and A. Tokmakoff, Phys. Rev. Lett. **86**, 2154 (2001).
[34]P. Hamm and M. Zanni, *Concepts and Methods of 2D Infrared Spectroscopy* (Cambridge University Press, 2011).
[35]S. W. Peterson and H. A. Levy, Acta Crystallogr. **10**, 70 (1957).
[36]G. Tammann, Annalen der Physik **307**, 1 (1900).
[37]G. Tammann, *Kristallisieren und Schmelzen: Ein Beitrag zur Lehre der Änderungen des Aggregatzustandes* (University of Tartu, 1903).
[38]W. B. McKinnon, "Geodynamics of icy satellites," in *Solar System Ices* (Springer Netherlands, 1998), pp. 525–550.
[39]A. D. Fortes, I. G. Wood, M. Alfredsson, L. Vočadlo, and K. S. Knight, J. Appl. Crystallogr. **38**, 612 (2005).
[40]P. W. Bridgman, Proc. Am. Acad. Arts. Sci. **47**, 441 (1912).
[41]P. W. Bridgman, J. Chem. Phys. **3**, 597 (1935).
[42]B. Kamb, Acta Crystallogr. **17**, 1437 (1964).
[43]B. Kamb, W. C. Hamilton, S. J. LaPlaca, and A. Prakash, J. Chem. Phys. **55**, 1934 (1971).
[44]C. Lobban, J. L. Finney, and W. F. Kuhs, J. Chem. Phys. **117**, 3928 (2002).
[45]T. Nakamura, M. Matsumoto, T. Yagasaki, and H. Tanaka, J. Phys. Chem. B **120**, 1843 (2016).
[46]C. G. Salzmann, P. G. Radaelli, A. Hallbrucker, E. Mayer, and J. L. Finney, Science **311**, 1758 (2006).
[47]B. Kamb, A. Prakash, and C. Knobler, Acta Crystallogr. **22**, 706 (1967).
[48]C. Lobban, J. L. Finney, and W. F. Kuhs, J. Chem. Phys. **112**, 7169 (2000).
[49]C. G. Salzmann, A. Hallbrucker, J. L. Finney, and E. Mayer, Phys. Chem. Chem. Phys. **8**, 3088 (2006).
[50]C. G. Salzmann, P. G. Radaelli, J. L. Finney, and E. Mayer, Phys. Chem. Chem. Phys. **10**, 6313 (2008).
[51]J. J. Shephard and C. G. Salzmann, Chem. Phys. Lett. **637**, 63 (2015).
[52]C. G. Salzmann, B. Slater, P. G. Radaelli, J. L. Finney, J. J. Shephard, M. Rosillo-Lopez, and J. Hindley, J. Chem. Phys. **145**, 204501 (2016).
[53]J. E. Bertie and B. F. Francis, J. Chem. Phys. **72**, 2213 (1980).
[54]B. Šukarova, W. F. Sherman, and G. R. Wilkinson, J. Mol. Struct. **79**, 289 (1982).
[55]G. E. Walrafen, M. Abebe, F. A. Mauer, S. Block, G. J. Piermarini, and R. Munro, J. Chem. Phys. **77**, 2166 (1982).
[56]B. Minčeva-Šukarova, W. F. Sherman, and G. R. Wilkinson, J. Phys. C **17**, 5833 (1984).
[57]B. Minčeva-Šukarova, G. E. Slark, and W. F. Sherman, J. Mol. Struct. **143**, 87 (1986).
[58]K. R. Hirsch and W. B. Holzapfel, J. Chem. Phys. **84**, 2771 (1986).
[59]C. Salzmann, I. Kohl, T. Loerting, E. Mayer, and A. Hallbrucker, J. Phys. Chem. B **106**, 1 (2002).
[60]C. G. Salzmann, I. Kohl, T. Loerting, E. Mayer, and A. Hallbrucker, J. Phys. Chem. B **107**, 2802 (2003).
[61]C. G. Salzmann, A. Hallbrucker, J. L. Finney, and E. Mayer, Chem. Phys. Lett. **429**, 469 (2006).
[62]T. Shigenari and K. Abe, J. Chem. Phys. **136**, 174504 (2012).
[63]J. E. Bertie and E. Whalley, Spectrochim. Acta **20**, 1349 (1964).
[64]J. E. Bertie and E. Whalley, J. Chem. Phys. **40**, 1646 (1964).
[65]J. E. Bertie, H. J. Labbé, and E. Whalley, J. Chem. Phys. **49**, 2141 (1968).
[66]V. F. Petrenko and R. W. Whithworth, *Physics of Ice* (Oxford University Press, 1999).
[67]J. Helbing and P. Hamm, J. Opt. Soc. Am. B **28**, 171 (2011).
[68]P. Hamm, R. A. Kaindl, and J. Stenger, Opt. Lett. **25**, 1798 (2000).
[69]R. Bloem, S. Garrett-Roe, H. Strzalka, P. Hamm, and P. Donaldson, Opt. Express **18**, 27067 (2010).
[70]D. van der Spoel, E. Lindahl, B. Hess, G. Groenhof, A. E. Mark, and H. J. C. Berendsen, J. Comput. Chem. **26**, 1701 (2005).
[71]H. J. C. Berendsen, J. R. Grigera, and T. P. Straatsma, J. Phys. Chem. **91**, 6269 (1987).
[72]T. Darden, D. York, and L. Pedersen, J. Chem. Phys. **98**, 10089 (1993).
[73]B. Hess, H. Bekker, H. J. C. Berendsen, and J. G. E. M. Fraaije, J. Comput. Chem. **18**, 1463 (1997).
[74]M. M. Conde, M. A. Gonzalez, J. L. F. Abascal, and C. Vega, J. Chem. Phys. **139**, 154505 (2013).
[75]M. Parrinello and A. Rahman, J. Appl. Phys. **52**, 7182 (1981).
[76]G. Bussi, D. Donadio, and M. Parrinello, J. Chem. Phys. **126**, 014101 (2007).
[77]B. Auer, R. Kumar, J. R. Schmidt, and J. L. Skinner, Proc. Natl. Acad. Sci. U. S. A. **104**, 14215 (2007).
[78]F. Li and J. L. Skinner, J. Chem. Phys. **132**, 204505 (2010).
[79]T. L. C. Jansen, D. Cringus, and M. S. Pshenichnikov, J. Phys. Chem. A **113**, 6260 (2009).
[80]C. Liang and T. L. C. Jansen, J. Chem. Theory Comput. **8**, 1706 (2012).
[81]B. Santra, J. Klimeš, A. Tkatchenko, D. Alfè, B. Slater, A. Michaelides, R. Car, and M. Scheffler, J. Chem. Phys. **139**, 154702 (2013).
[82]H. Iglev, M. Schmeisser, K. Simeonidis, A. Thaller, and A. Laubereau, Nature **439**, 183 (2006).
[83]A. Dokter and H. Bakker, J. Chem. Phys. **128**, 024502 (2008).
[84]T. Steinel, J. B. Asbury, J. Zheng, and M. D. Fayer, J. Phys. Chem. A **108**, 10957 (2004).
[85]Y. L. A. Rezus and H. J. Bakker, J. Chem. Phys. **123**, 114502 (2005).
[86]J. R. Scherer and E. G. Snyder, J. Chem. Phys. **67**, 4794 (1977).
[87]Q. Shi and E. Geva, J. Chem. Phys. **129**, 124505 (2008).
[88]S. Knop, T. L. C. Jansen, J. Lindner, and P. Vöhringer, Phys. Chem. Chem. Phys. **13**, 4641 (2011).
[89]K. Kwac and E. Geva, J. Phys. Chem. B **116**, 2856 (2012).
[90]C. P. van der Vegte, S. Knop, P. Vöhringer, J. Knoester, and T. L. C. Jansen, J. Phys. Chem. B **118**, 6256 (2014).
[91]J. Edler and P. Hamm, J. Chem. Phys. **119**, 2709 (2003).